








Magnetic properties of Ni₅Sn(O₂BO₃)₂ ludwigiteC. P. C. Medrano ^{1,2,*}, E. Sadrollahi^{3,4}, R. G. M. Da Fonseca ⁵, E. C. Passamani ⁶, D. C. Freitas ², M. A. Continentino ¹,
D. R. Sanchez ², F. J. Litterst^{1,3} and E. Baggio-Saitovitch ¹¹*Centro Brasileiro de Pesquisas Físicas, Rua Doutor Xavier Sigaud, 150-Urca, 22290-180 Rio de Janeiro, Rio de Janeiro, Brazil*²*Instituto de Física, Universidade Federal Fluminense, Campus da Praia Vermelha, 24210-346 Niterói, Rio de Janeiro, Brazil*³*Institut für Physik der Kondensierten Materie, Technische Universität Braunschweig, 38106 Braunschweig, Germany*⁴*Institut für Festkörper- und Materialphysik, Technische Universität Dresden, 01069 Dresden, Germany*⁵*Department of Physics, Federal University of São Carlos, São Carlos, São Paulo, Brazil*⁶*Departamento de Física, Universidade Federal do Espírito Santo, 29075-910 Vitória, Espírito Santo, Brazil*

(Received 29 September 2020; revised 22 December 2020; accepted 8 February 2021; published 24 February 2021)

The magnetic properties of site-disordered Ni₅Sn(O₂BO₃)₂ ludwigite have carefully been studied using local probes and bulk experimental methods in temperatures down to 1.6 K and magnetic fields up to 9 T. Our results have clearly shown the role of the effect of order/disorder site occupancy in these complex compounds with spin moments $S = 1$. Different from most ludwigites, site-disordered Ni₅Sn(O₂BO₃)₂ ludwigite has shown three magnetic transitions at 80, 50, and 5 K. Local probes (¹¹⁹Sn Mössbauer and muon spin spectroscopy) have indicated a partial long-range magnetic order with onsets at 80 and 50 K with predominant ferromagnetic interactions at 80 K and antiferromagnetic ones at 50 K. At lower temperatures, a partial spin-glass-like freezing of the moments has been developed concomitantly with fraction of the moments ordered at higher temperatures, a spin-glass-like and long-range magnetic order coexist and a spontaneous exchange bias effect has been observed. Applied magnetic fields have gradually reduced magnetic frustration, leading to a magnetically ordered state of the complete structure at 51 K under 9 T. The absence of double-exchange interactions in order/disorder Ni₅Sn(O₂BO₃)₂ ludwigites shows how the magnetic interactions that compete as direct exchange and double exchange are modified by the site occupancy of nonmagnetic Sn ions. Features as a third magnetic transition, the appearance of spontaneous exchange bias, and the enhancement of the coercive field at low temperatures were not found in the site-ordered isomer compound.

DOI: [10.1103/PhysRevB.103.064430](https://doi.org/10.1103/PhysRevB.103.064430)**I. INTRODUCTION**

Magnetic oxyborates of the 3d transition metals have complex and intriguing physical properties. They are good examples of strongly correlated systems in which magnetic frustration and structural disorder have often been observed [1]. Low-dimensional substructures are characteristic on these compounds, and they are present in the form of ladders in ludwigites, ribbons in warwickites, and planes in hulsites.

Ludwigites have the general formula $M_2^{2+}M'^{3+}O_2BO_3$, where M, M' are transition metals occupying four sites in the orthorhombic structure, see Fig. 1(a). The boron ions (green spheres) have trigonal coordination. This structure is usually represented as forming two low-dimensional subunits in the form of three-leg ladders, the 4-2-4, and the 3-1-3 ladders as schematically represented in Fig. 1(b). Ladder 3-1-3 is occupied by M^{2+} ions, whereas ladder 4-2-4 is usually occupied by $M'^{3+}-M^{2+}-M'^{3+}$ ions in the rung and has the shortest intermetallic distance between sites 2 and 4, conferring different structural and magnetic properties to these substructures. Different metal ions and valence states are allowed and, generally, there is a competition among direct, double exchange, and

superexchange interactions, which lead to complex magnetic structures.

The only two homometallic Fe₃O₂BO₃ and Co₃O₂BO₃ ludwigites have rather different properties. For instance, Fe₃O₂BO₃ shows multiferroic properties, a charge-ordering transition related to ladder 4-2-4, that is solely occupied by three Fe³⁺ ions in the rung with one “extra” itinerant electron that, at 283 K, favors a charge-density wave along the c axis. In addition, ladders 4-2-4 and 3-1-3 order independently at 112 and 70 K, respectively, in orthogonal directions [2–6]. A similar orthogonal arrangement of spins in the ladder was observed in Fe_{3-x}Mn_xO₂BO₃ ludwigites [7]. In contrast, a rather different behavior was measured in Co₃O₂BO₃ ludwigite [8–10]. Here electrons are localized, ladder 4-2-4 is occupied by Co³⁺-Co²⁺-Co³⁺ ions, full magnetic order of the compound at 42 K with spins pointing along the b axis, and Co³⁺ ions in low spin state ($S = 0$) give rise to a two-dimensional- (2D-) like magnetic structure formed by sites 2, 3, and 1. Furthermore, this compound has shown an important oxygen evolution reaction in hybrid form with reduced-multiwalled carbon nanotubes for electrocatalysis [11]. The substitution of Co-based ludwigites by nonmagnetic ions has enhanced their magnetic properties, for example, increasing the long-range magnetic-order temperature to 57 K [82 K] in the Co_{0.76}Al_{1.24}(O₂BO₃)₂

*ccontreras@cbpf.br, ccontreras@id.uff.br

[12] $[\text{Co}_5\text{Sn}(\text{O}_2\text{BO}_3)_2]$ [13] compound. Besides that, the substitution leads to an improvement of magnetocaloric properties of $\text{Co}_{4.76}\text{Al}_{1.24}(\text{O}_2\text{BO}_3)_2$ and provokes metamagnetic phase transitions for both nonmagnetic-doped compounds. Spin-glass-like behavior was also found in $\text{Co}_5\text{Ti}(\text{O}_2\text{BO}_3)_2$ [14] and $\text{CoMgGaO}_2\text{BO}_3$ [15].

According to literature there is no homometallic Ni-based ludwigite, but heterometallic Ni-based ludwigites with magnetic ions have shown magnetic order of Fe ions at ~ 107 K and a spin freezing of the Ni ions at ~ 46 K in $\text{Ni}_2\text{FeO}_2\text{BO}_3$ [16,17]. A pole reversal of magnetization was found in $\text{Ni}_2\text{MnO}_2\text{BO}_3$ [18,19]. Ni-based ludwigites containing nonmagnetic ions display an antiferromagnetic order in $\text{Ni}_2\text{AlO}_2\text{BO}_3$ [20] and $\text{Ni}_5\text{Ti}(\text{O}_2\text{BO}_3)_2$ [21]. A partial magnetic order and/or spin-glass-like state could not be well distinguished below 70 K in $\text{Ni}_5\text{Ge}(\text{O}_2\text{BO}_3)_2$ [22] and site-ordered $\text{Ni}_5\text{Sn}(\text{O}_2\text{BO}_3)_2$ [23]. This latter compound had a particular ordered site occupancy of Sn at site 4 (*4h*).

Nonmagnetic ions are usually used to reduce magnetic interactions as an effort to understand these complex magnetic compounds [13]. However, heterometallic ludwigites with different nonmagnetic ions have displayed distinct properties, making it difficult to attribute if those changes are produced by the nonmagnetic ions (different orbitals or ionic radii) or by different structures (changes in site occupancy or in the interatomic distances). Consequently, knowing the changes produced by site order-disorder occupancy of nonmagnetic ions in isomer compounds performs a step ahead in the study of these compounds.

Thus, in this paper, we present a thorough investigation of the effect of site-disorder occupancy of ladder 4-2-4 on the low-temperature magnetic properties of $\text{Ni}_5\text{Sn}(\text{O}_2\text{BO}_3)_2$ ludwigite using local probe and bulk experimental methods, including ^{119}Sn Mössbauer and muon spin spectroscopy, AC and DC magnetization on powder and oriented crystals, heat capacity down to 1.6 K, and under applied fields up to 9 T. These different measurements distinguish three magnetic anomalies in the magnetic and specific-heat measurements. The results indicate a partial long-range magnetic order of the 4-2-4 ladder below 80 K with predominant ferromagnetic interactions, and it changes to predominant antiferromagnetic interactions below 50 K. At lowest temperatures, spin-glass-like freezing of the moments and large magnetic frustration are observed in coexistence with a long-range order. Applied magnetic fields reduce magnetic frustration, and the magnetic order of the whole system appears to take place under a field of 9 T at 51 K.

II. EXPERIMENT

A. Synthesis

Dark-green needle crystals of $\text{Ni}_5\text{Sn}(\text{O}_2\text{BO}_3)_2$ ludwigite were synthesized from a 5:1:2 molar mixture of $\text{NiO}_2:\text{SnO}_2:\text{H}_3\text{BO}_3$ with a large excess of borax. The mixture was heated at 1160°C for 30 min and cooled down to 600°C in 24 h. Then, the oven was turned off. The bath was dissolved in hot water, and the crystals washed in diluted hydrochloric acid. The same thermal treatment and molar mixture were used for the synthesis of $\text{Ni}_{5.15}\text{Sn}_{0.85}(\text{O}_2\text{BO}_3)_2$ hulsite as re-

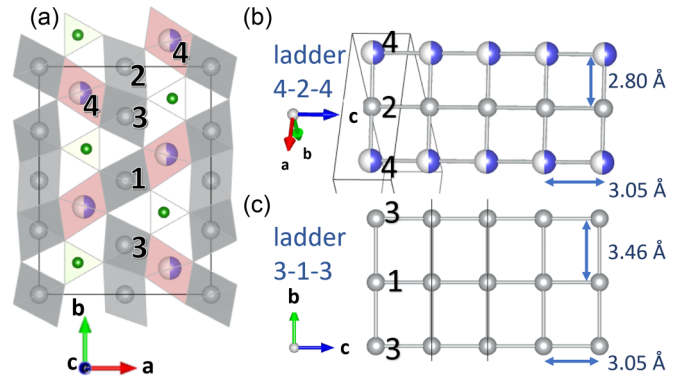


FIG. 1. Schematic of ludwigite compounds. (a) Projected along the *c* axis. The octahedra formed by oxygen atoms centered on the metal ions are shown. Ladders 4-2-4 and 3-1-3 along the *c* axis are presented in (b) and (c) panels, respectively, and interatomic distances are presented for site-disordered $\text{Ni}_5\text{Sn}(\text{O}_2\text{BO}_3)_2$ ludwigite. This picture is made by VESTA 3.1.1 software [25].

ported in Ref. [1]. Different borax saturations were needed to get the two structures, here only 1/3 of the borax quantity was employed. The purity of the sample was confirmed by x-ray powder and single-crystal diffractions.

B. Structural characterization

X-ray diffraction was performed on a needle single crystal. The measurement was carried out with a D8 Venture Bruker diffractometer, operating at room temperature using $\text{I}\mu\text{S}$ microfocus x-ray $\text{Mo K}\alpha$ radiation. The details on refinement and crystallographic data of $\text{Ni}_5\text{Sn}(\text{O}_2\text{BO}_3)_2$ are reported in the Supplemental Material [24].

Site-disordered $\text{Ni}_5\text{Sn}(\text{O}_2\text{BO}_3)_2$ ludwigite crystallizes in the orthorhombic space-group *Pbam*. The schematic is shown in Fig. 1(a), sites 2, 3, and 1 in gray color are exclusively occupied by Ni atoms, and site 4 in pink is randomly occupied by Ni and Sn atoms. Fractional coordinates and main bond lengths in this compound are in the Supplemental Material [24] (see also Refs. [26,27] therein). The random occupation of Ni and Sn ions on site 4 in the present system is different from $\text{Ni}_5\text{Sn}(\text{O}_2\text{BO}_3)_2$ ludwigite of Ref. [23], which has an ordered occupation of Sn atoms along the *c* axis, an effect that can be explained considering the different synthesis processes. This difference in Ni and Sn site occupations is reflected in the unit-cell parameter *c* and the crystallographic space group changing from $c \sim 3$ Å and space-group *Pbam* ($N^\circ 55$) in the former to $c \sim 6$ Å and space-group *Pnma* ($N^\circ 62$) in the latter, see Fig. 2(c).

C. Magnetic measurements

The magnetization measurements of $\text{Ni}_5\text{Sn}(\text{O}_2\text{BO}_3)_2$ ludwigite were performed on both powder and oriented single crystals using a commercial Quantum Design physical property measurement system (PPMS) and superconducting quantum interference device-vibrating sample magnetometer equipment, respectively. The results of the magnetic measurements are shown in Figs. 3–5.

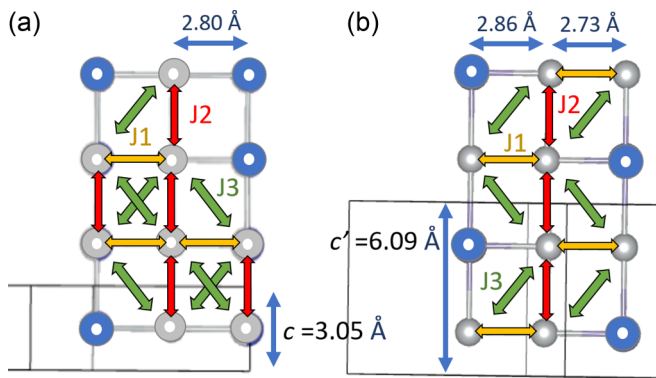


FIG. 2. Comparative scheme of site occupancy of Ni and Sn atoms in gray and blue respectively, in ladder 4-2-4 of $\text{Ni}_5\text{Sn}(\text{O}_2\text{BO}_3)_2$ ludwigite: (a) site disordered and (b) site ordered. Magnetic exchange paths are illustrated with different colors.

Special care was given to the demagnetization process. A “magnet reset” process was performed previous to each ZFC measurement to prevent remnant fields. Figure 3 displays magnetization measurements in oriented crystals with an applied magnetic field of 100 Oe along and perpendicular to the c axis. The magnetization response at low temperatures has a stepwise fashion as seen in the inset of Fig. 3. The steps are observed below 80 K with a larger increase below 60 K. ZFC and FC curves increase below the magnetic transition, but below 10 K, they reach a plateau. In $\text{Ni}_5\text{Sn}(\text{O}_2\text{BO}_3)_2$ ludwigite, the plateau of the ZFC curves at low temperatures is also observed in measurements under 200 and 1000 Oe and on a sample of ground single crystals under 200 Oe. Different batches show reproducible behavior. Oriented crystals show the anisotropic magnetic susceptibility response. The easy

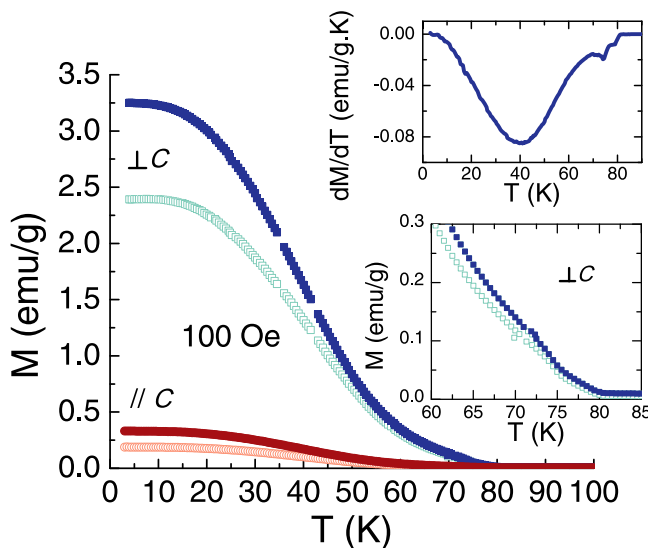


FIG. 3. $\text{Ni}_5\text{Sn}(\text{O}_2\text{BO}_3)_2$ ludwigite magnetization versus temperature under a probe magnetic field of 100 Oe in both protocols: field cooled [(FC), dark color] and zero-field cooled [(ZFC), light color] for oriented crystals. The $\perp c$ axis is in blue and the $\parallel c$ axis is in red. The upper inset shows the derivatives dM/dT versus T of the FC $\perp c$ axis. The lower inset is a zoomed figure of the data $\perp c$ axis.

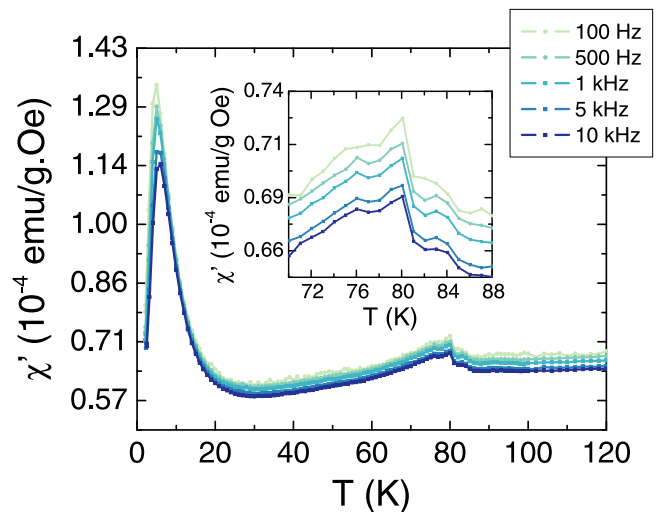


FIG. 4. Real part of the AC susceptibility for $\text{Ni}_5\text{Sn}(\text{O}_2\text{BO}_3)_2$ as a function of temperature for 0.1, 0.5, 1, 5, and 10 kHz. The inset shows a zoomed-up plot around 80 K.

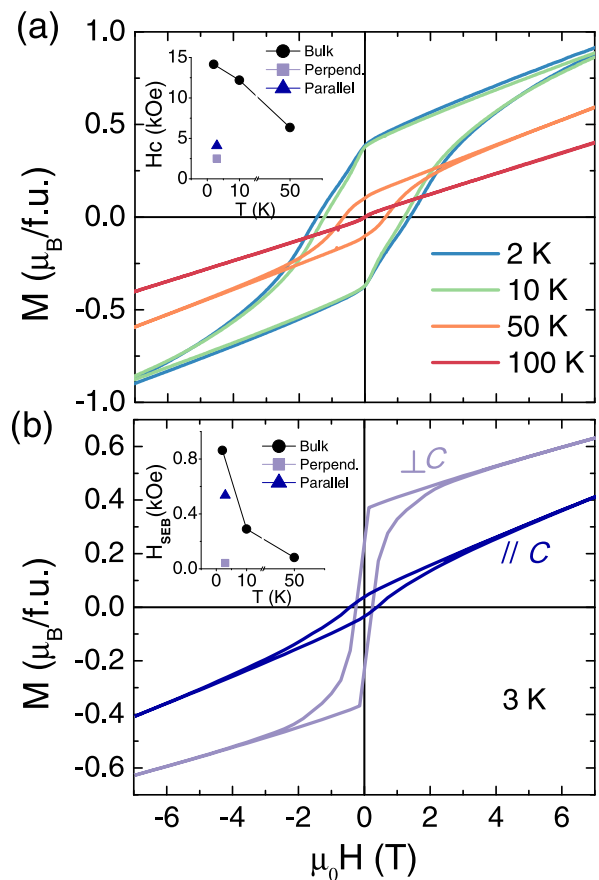


FIG. 5. $\text{Ni}_5\text{Sn}(\text{O}_2\text{BO}_3)_2$ magnetization versus applied magnetic-field curves. (a) For grounded single crystals at 2, 10, 50, and 100 K. The inset shows coercive fields. (b) For the oriented crystal along and perpendicular to the c axis at 3 K. The inset shows the spontaneous exchange bias fields.

magnetization direction is on the a - b plane as also observed in $\text{Ni}_5\text{Ge}(\text{O}_2\text{BO}_3)_2$ ludwigite [23].

From the linear fit of the inverse DC susceptibility (FC-1 T perpendicular to the c axis, not shown) above 200 K, we obtained a Curie-Weiss temperature $\theta_{\text{CW}} = -82.8$ K and a Curie constant $C = 6.12 \times 10^{-3} \text{ emu K}^{-1} \text{ g}^{-1} \text{ Oe}^{-1}$. The negative value of θ_{CW} indicates the predominance of antiferromagnetic interactions. From the Curie constant, an effective moment per formula unit (f.u.) $p_{\text{eff}} = 5.28\mu_B$ is determined. The spin only moment per f.u. of $\text{Ni}_5\text{Sn}(\text{O}_2\text{BO}_3)_2$ with $S = 1$ is $p = 6.32\mu_B$, i.e., the measured effective moment is lower than the pure spin contribution in this compound. Two main effects could be responsible for the reduction of the moment: Crystal field or a partial magnetic order. The former, in general, is responsible for small deviations, whereas the latter would result in the observed drastic reduction of moment. In fact, a similar behavior was observed in $\text{Ni}_{5.15}\text{Sn}_{0.85}(\text{O}_2\text{BO}_3)_2$ hulsite with a partial magnetic order of the planar substructure with rectangular arrangement of Ni ions, whereas the other substructure, formed by a triangular arrangement of Ni atoms, does not order down to 3 K [1]. In addition, the lower value of the effective moment with respect to the one calculated for a spin only contribution is not characteristic of magnetic frustrations. Even in Ni compounds with a large magnetic frustration as the spin liquid candidates $6H$ - B and $3C$ phases of $\text{Ba}_3\text{NiSb}_2\text{O}_9$, the effective moment corresponds to typical values of Ni^{2+} ions [28].

Figure 4 shows the real part of the AC-susceptibility (χ') for different frequencies as a function of temperature. When the temperature is reduced, the susceptibility remains almost equal until 85 K when small increases are observed again in a stepwise fashion, describing a broad transition. Below 76 K, the susceptibility decreases down to 25 K reaching smaller values than those above 85 K. Below 25 K, a second increase starts, describing a large peak (the intensity is almost ten times the one observed below 85 K) with maximum at 5 K. The variation of this peak with frequency for two decades is smaller than 2 K. This peak temperature corresponds to the plateau in the DC magnetization (Fig. 3). It is better seen from the inset of Fig. 3 with a zero value of the derivative of magnetization. Thus, the susceptibility response of this site-disordered compound is rather different from that observed on site-ordered $\text{Ni}_5\text{Sn}(\text{O}_2\text{BO}_3)_2$, which has one peak at 73 K and a broad second peak at around 15 K yet less intense [23].

Figure 5 presents the $M(H)$ loops for the grounded and oriented single crystals. Hysteresis curves have been observed below 100 K [see Fig. 5(a)], which is consistent with a ferromagneticlike order. Note that at 50 K, the shape, the remnant magnetization, and the coercive field values of the loop are similar to the ones observed for $\text{Ni}_5\text{Ti}(\text{O}_2\text{BO}_3)_2$ at 4.5 K [21]. At 10 K, the $M(H)$ loop opens more, the remnant magnetization is four times larger, and the coercive field is about twice larger than at 50 K. At 2 and 10 K, $M(H)$ loops are quite similar. The value of the remnant magnetic field is the same as that observed in site-ordered $\text{Ni}_5\text{Sn}(\text{O}_2\text{BO}_3)_2$, but the coercive field is largely increased. Figure 5(b) shows the $M(H)$ loops in oriented single crystals of $\text{Ni}_5\text{Sn}(\text{O}_2\text{BO}_3)_2$ ludwigite at 3 K. These curves have open loop characteristics of a ferromagneticlike behavior, however, saturation is not reached up to 7 T. On the other hand, the

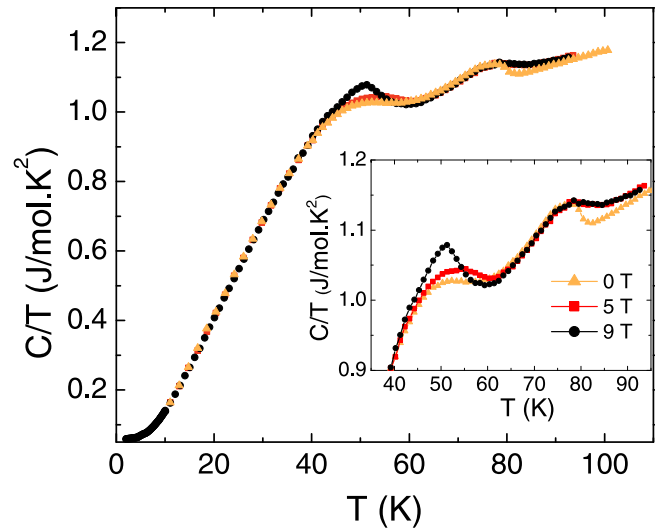


FIG. 6. Specific heat of $\text{Ni}_5\text{Sn}(\text{O}_2\text{BO}_3)_2$ ludwigite, plotted as C/T versus T for applied magnetic fields of 0, 5, and 9 T. The inset: Zoom of the peaks between 35 and 95 K.

hysteresis curve perpendicular to the c axis has not only the shape, but also the remnant magnetization and coercive field values similar to those observed for powder measurement of site-ordered $\text{Ni}_5\text{Sn}(\text{O}_2\text{BO}_3)_2$ ludwigite reported in Ref. [23]. Spontaneous exchange bias effects (horizontal shifting of the $M(H)$ curves along the field axis [29]) are observed, see the inset of Fig. 5(b). Hysteresis loops of oriented single crystals of $\text{Ni}_5\text{Sn}(\text{O}_2\text{BO}_3)_2$ and $\text{Co}_5\text{Sn}(\text{O}_2\text{BO}_3)_2$ ludwigites under applied magnetic fields are presented in the Supplemental Material [24] to compare their magnetic responses. Magnetic anisotropy on the plane perpendicular to the c axis is a common characteristic of these samples. However, for $\text{Co}_5\text{Sn}(\text{O}_2\text{BO}_3)_2$, the magnetization is practically saturated in both directions, whereas for $\text{Ni}_5\text{Sn}(\text{O}_2\text{BO}_3)_2$ the magnetization increases linearly with the magnetic field. This behavior is consistent with a partial magnetic order as discussed below.

D. Specific heat

Specific-heat measurements as a function of temperature and magnetic field were performed with a pellet sample of $\text{Ni}_5\text{Sn}(\text{O}_2\text{BO}_3)_2$ ludwigite in the temperature range of $2 \text{ K} \leq T \leq 100 \text{ K}$ using a commercial Quantum Design Dynacool (PPMS).

Figure 6 shows the specific-heat curves plotted as C/T versus T for applied magnetic fields of 0, 5, and 9 T. As expected for solid materials, there is a continuous reduction of the specific-heat values as the sample temperature is decreasing, which for this compound becomes steeper below 50 K. In addition, there also are two oscillations in the specific-heat curves at about 80 and 50 K, which are field dependent. The one at 80 K corresponds to the temperature region where an anomaly is observed in the AC and DC magnetization experiments. The intensity of the peak is reduced with applied magnetic fields (see the inset), supporting the predominance of ferromagnetic interactions. A second increase in the specific heat occurs at ~ 60 K, reaching a maximum at 50 K. The application of a magnetic field of 5 T slightly moves the peaks

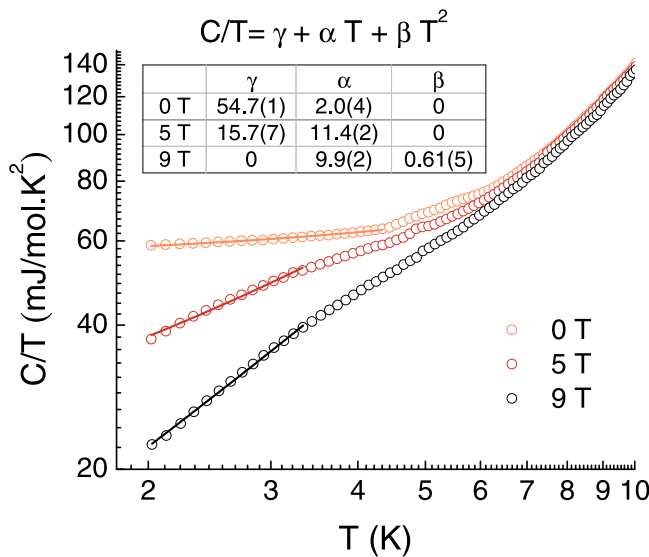


FIG. 7. Low-temperature specific heat versus temperature of $\text{Ni}_5\text{Sn}(\text{O}_2\text{BO}_3)_2$ ludwigite. The lines through the data are fittings to a power-law $C/T = \gamma + \alpha T + \beta T^2$.

to higher temperatures. However, an applied magnetic field of 9 T increases the peak at 51 K and narrows it. As observed in other ludwigite compounds, applied magnetic fields may widen and reduce specific-heat peaks. This particular shape of peak (after application of a large magnetic field) suggests that a different type of magnetic order is formed and indicates the predominance of antiferromagnetic order in this temperature range.

Figure 7 displays the low-temperature specific-heat curves plotted as C/T versus T for 0, 5, and 9 T. The curve at 0 T has a change in the slope above 4 K that could correspond to the peak observed at 5 K in the AC susceptibility (Fig. 4). The low-temperature data were fitted with $C/T = \gamma + \alpha T + \beta T^2$, and the fitting parameters are given in the table inside Fig. 7. The fit of the 0-T curve gives a dominant linear term (γ). The here observed value [$\gamma(0 \text{ T}) = 54.7(1) \text{ mJ mol}^{-1} \text{ K}^{-2}$] is larger than that observed in the $\text{Ni}_5\text{Ti}(\text{O}_2\text{BO}_3)_2$ [$\gamma(0 \text{ T}) = 2.26 \text{ mJ mol}^{-1} \text{ K}^{-2}$] and in the $\text{Co}_5\text{Ti}(\text{O}_2\text{BO}_3)_2$ [$\gamma(0 \text{ T}) = 15.5 \text{ mJ mol}^{-1} \text{ K}^{-2}$] in which the whole structure displays a spin-glass-like transition, Ref. [14]. This also indicates a strong magnetic frustration in $\text{Ni}_5\text{Sn}(\text{O}_2\text{BO}_3)_2$. For an applied magnetic field of 9 T, the T^2 term (α) becomes dominant, reducing drastically the γ term, indicating a loss of magnetic frustration. This unexpected T^2 dependence in $\text{Ni}_5\text{Sn}(\text{O}_2\text{BO}_3)_2$ could be an indication for 2D-like antiferromagnetic magnons and phonons as met in $\text{Co}_{4.76}\text{Al}_{1.24}(\text{O}_2\text{BO}_3)_2$ [12].

E. Mössbauer spectroscopy

^{119}Sn Mössbauer absorption spectra were performed in transmission geometry using a standard spectrometer with a sinusoidal velocity sweep. The $^{119m}\text{Sn}:\text{CaSnO}_3$ source was kept at room temperature. The samples of $\text{Ni}_5\text{Sn}(\text{O}_2\text{BO}_3)_2$ were mounted in a Montana variable temperature closed-cycle cryostat. The sample temperature was varied between 3 and

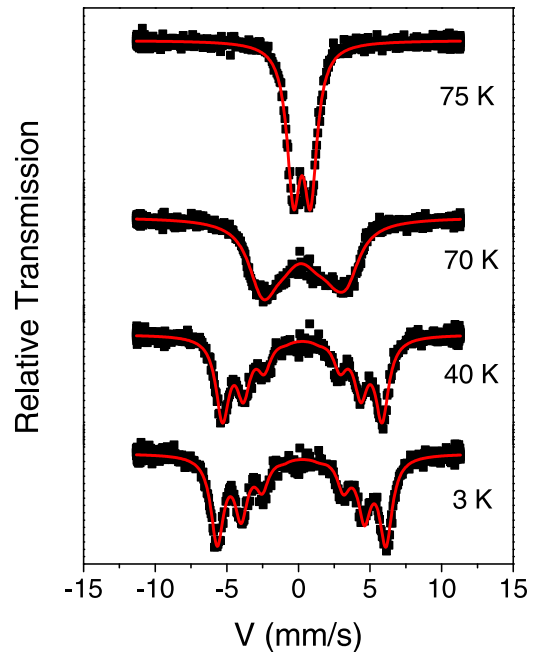


FIG. 8. ^{119}Sn Mössbauer spectra of $\text{Ni}_5\text{Sn}(\text{O}_2\text{BO}_3)_2$ ludwigite in the temperature range of $3 \text{ K} \leq T \leq 75 \text{ K}$.

300 K. The least-squares fitting program software MOSSWINN [30] was used for analyzing the spectra. Some representative ^{119}Sn Mössbauer spectra for the $\text{Ni}_5\text{Sn}(\text{O}_2\text{BO}_3)_2$, taken at several temperatures, are shown in Fig. 8.

The obtained hyperfine parameters are given in Table I. The magnetic hyperfine field at the Sn nucleus is a transferred magnetic field, resulting from the magnetic moments of the neighboring Ni ions [31]. The center shift (CS) values are given relative to the source CaSnO_3 . The room-temperature spectrum presents a single doublet with $\text{CS} = 0.26 \text{ mm/s}$, consistent with an oxidation state 4+ for Sn [31]. The linewidth W of about 1 mm/s indicates that Sn ions are positioned at only one site, in agreement with the x-ray data discussed above (no spurious phase was detected). The spectra between 200 and 75 K can be fitted using only one paramagnetic doublet.

Below 75 K, the spectra reveal a magnetic hyperfine splitting, see Fig. 8, indicating the onset of magnetic order. This temperature is slightly lower than the temperature at which the susceptibility increases. The Mössbauer spectra were fitted using a hyperfine Hamiltonian comprising the magnetic hyperfine interaction and the nuclear electric quadrupole interaction (see Table I). The quadrupole splitting in the paramagnetic regime $\Delta E_Q = eV_{zz}Q\sqrt{1 + \eta^2}/3$ is $1.13(2) \text{ mm/s}$ (e is the elementary charge, V_{zz} is the electrical-field gradient main component at Sn, Q is the nuclear quadrupole moment of ^{119}Sn excited nuclear spin state $I = 3/2$). From this splitting, it is not possible to determine neither the sign of the electrical-field gradient nor the asymmetry parameter η describing the deviation from axial symmetry. This becomes possible in the magnetically ordered regime. Assuming no structural changes to occur below 200 K, we kept the value of $eV_{zz}Q$ independent of temperature. The fits of the magnetic patterns show that it is, in fact, negative $= -1.09 \text{ mm/s}$

TABLE I. Mössbauer hyperfine parameters of $\text{Ni}_5\text{Sn}(\text{O}_2\text{BO}_3)_2$. The parameters are CS, quadrupole splitting ΔE_Q , the electric-field gradient main component V_{zz} , the asymmetry parameter η , hyperfine magnetic-field B_{hf} , angle θ between the B_{hf} and the electric-field gradient main axis, and linewidth W .

T (K)	CS (mm/s)	ΔE_Q (mm/s)	V_{zz}	η	θ (deg)	B_{hf} (T)	W (mm/s)
200	0.24(5)	1.13(2)					1.11(5)
75	0.25(5)	1.13(2)					1.12(5)
70	0.30(5)		13.1 ^a	0.51(5)	90(2)	4.29(5)	2.26(5)
60	0.28(5)		13.1 ^a	0.61(5)	79(2)	6.79(5)	1.33(5)
50	0.30(5)		13.1 ^a	0.56(5)	72(2)	7.72(5)	1.19(5)
40	0.33(5)		13.1 ^a	0.58(5)	66(2)	8.19(5)	1.11(5)
30	0.26(5)		13.1 ^a	0.56(5)	61(2)	8.56(5)	1.12(5)
20	0.26(5)		13.1 ^a	0.49(5)	58(2)	8.63(5)	1.14(5)
3	0.26(5)		13.1 ^a	0.45(5)	58(2)	8.66(5)	1.06(5)

^aMeans fixed value.

(i.e., $V_{zz} = 13.1 \times 10^{21} \text{ V/m}^2$). The values of the asymmetry parameter η are about 0.5, which is in good agreement with ΔE_Q found in the paramagnetic state. Such a deviation from axial symmetry indicated by the nonzero value of η is to be expected due to the orthorhombic structure. B_{hf} increases with decreasing temperature following a typical magnetization curve, reaching saturation at 30 K. The presence of a single magnetic component could, in principle, indicate a relatively simple magnetic structure. Figure 9 displays the normalized hyperfine magnetic field [$B_{hf}(T)/B_{hf}(3 \text{ K})$] as a function of reduced temperature ($T/T' = 75 \text{ K}$) of $\text{Ni}_5\text{Sn}(\text{O}_2\text{BO}_3)_2$, together with the normalized magnetization curves derived from a Brillouin function for $J = 1$ (blue solid line). These curves are close to the experimental data (black solid symbols), however, the system is not a classical ferromagnet. In fact, the negative Curie-Weiss temperature indicates that antiferromagnetic interactions are involved. The analysis of the Mössbauer spectra also reveals that angle θ between the magnetic hyperfine-field B_{hf} and the electrical-field gradient main axis is varying from about 90° at 70 K to about 60°

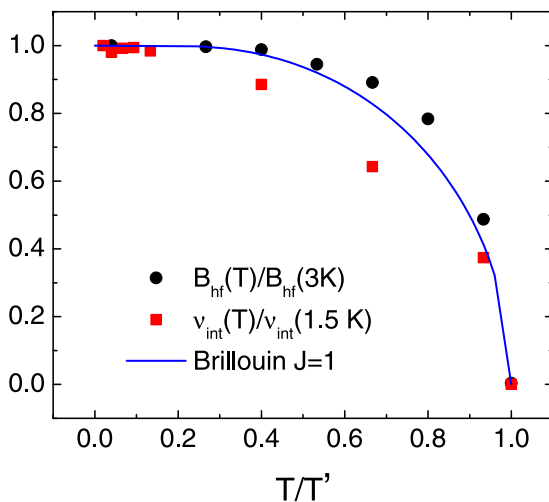


FIG. 9. Normalized hyperfine magnetic-field $B_{hf}(T)/B_{hf}(3 \text{ K})$ in black and normalized spontaneous muon spin rotation frequency $v_{\text{int}}(T)/v_{\text{int}}(T = 1.5 \text{ K})$ in red versus $T/T' = 75 \text{ K}$ of $\text{Ni}_5\text{Sn}(\text{O}_2\text{BO}_3)_2$ ludwigite. The solid line in blue corresponds to a Brillouin fit with $J = 1$.

at lower temperatures (see Table I), i.e., the spin structure changes below 70 K.

F. Muon spin rotation and relaxation

Muons spin rotation and relaxation (μSR) experiments on a powder specimen of $\text{Ni}_5\text{Sn}(\text{O}_2\text{BO}_3)_2$ ludwigite have been performed using the nearly 100% spin-polarized μ^+ beam of the πM3 beamline of the Paul Scherrer Institute in Villigen, Switzerland. Experiments were performed using the General Purpose Surface-Muon instrument with either a weak magnetic field of 5 mT applied perpendicular to the initial muon spin polarization [the weak Transverse Field (wTF) mode] or without the applied field [the Zero Field (ZF) mode]. The sample temperature could be varied between 1.6 and 300 K.

The purpose for performing μSR was to get additional information concerning the various magnetic changes traced by susceptibility (averaged over all samples) and the local view provided by the transferred magnetic hyperfine field at Sn. Despite the proper implantation site of μ^+ is not known, one can expect that it is close to an oxygen, thus, having a different view on the local magnetic scenario. From ZF experiments we can learn about the temperature-dependent development of local magnetic-fields B_μ in the long-range ordered regime, their static distribution, and eventual dynamics. wTF experiments are in our case especially suited for detecting the magnetic transitions and revealing eventual partial order.

In the experiments, the time-dependent asymmetries $A(t)$ of the decay positron count rates are recorded. From these, the time-dependent polarization of muon spins after implantation at time $t = 0$: $A(t)/A(0) = G_z(t)$ is derived.

In the paramagnetic state, the wTF polarization function will oscillate with a frequency $\nu_\mu = \gamma_\mu B_\mu / (2\pi)$. $\gamma_\mu = 135.54/\mu\text{s T}$ is the muon gyromagnetic ratio. Here B_μ corresponds to the applied-field B_{app} and an additional minor Knight-shift contribution. Upon onset of magnetic order, there appear additional local-fields B_μ that in a powder specimen will add at random directions to B_{app} . Since these B_μ 's are typically much larger than B_{app} , there will occur a severe damping of the wTF rotation signal leading to an apparent vanishing of this signal. In case the specimen is only partially ordered, there will still be left a signal rotating in B_{app} with an asymmetry corresponding to the paramagnetic volume

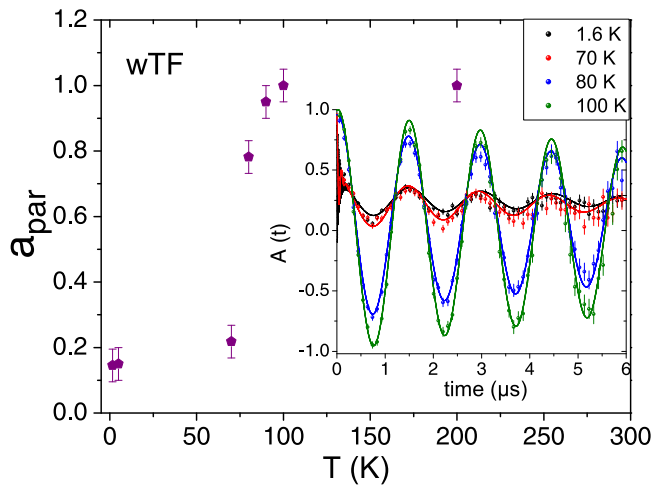


FIG. 10. Normalized rotation asymmetry [$a_{\text{par}}(T) = a_{\text{rot}}(T)/a_{\text{rot}}(T = 100 \text{ K})$] of the wTF spectra (inset) versus temperature of $\text{Ni}_5\text{Sn}(\text{O}_2\text{BO}_3)_2$ ludwigite.

fraction of the specimen. As shown in Fig. 10, there is a loss of rotation asymmetry around $T_{N1} = 80 \text{ K}$. The transition is not sharp, and the few temperatures at which experiments were performed are not sufficient to resolve the double transition proposed from the AC susceptibility experiment. At 70 K, we still have a residual asymmetry of about 25% of that found above T_{N1} at 1.6 K it is about 15%.

This latter signal contribution can be attributed, in part, to an undamped background signal from the sample holder. However, the larger rotating signal at 70 K indicates that this must also comprise some still paramagnetic volume fraction of the specimen. This becomes more apparent upon inspection of the ZF data.

In ZF, there appear spontaneous rotation signals (see Fig. 11) below T_{N1} . The ZF signals can be described by

$$G_z(t)^{\text{ZF}} = a_{\text{rot}} G_z(t)_{\text{rot}}^{\text{ZF}} + a_{\text{ge}} G_z(t)_{\text{ge}}^{\text{ZF}} + \text{BG}, \quad (1)$$

with

$$G_z(t)_{\text{rot}}^{\text{ZF}} = \frac{2}{3} e^{-\lambda_t t} \cos(2\pi \nu_{\text{int}} t) + \frac{1}{3} e^{-\lambda_l t}. \quad (2)$$

ν_{int} is the rotation frequency in local internal fields caused by ordered electronic moments, λ_t is the transverse damping parameter of the oscillations mainly caused by field inhomogeneities, the longitudinal damping λ_l of the “1/3 tail” is related to field fluctuations along the direction of initial muon polarization. a_{rot} is the partial asymmetry of the rotating signal.

The longitudinal damping factors λ_l can be kept fixed to zero, i.e., the rotation patterns are due to static fields. The transverse damping factor is large for all temperatures (see the Supplemental Material [24]), which means that the local fields at these muon sites have a wide distribution. The temperature dependence of the frequency $\nu_{\text{int}}(T)$ is presented in the Supplemental Material [24]. Yet, as can be seen from a normalized plot $\nu_{\text{int}}(T)/\nu_{\text{int}}(T = 1.6 \text{ K})$ shown in Fig. 9 together with the normalized transferred magnetic hyperfine fields measured at Sn, the muon spin rotation frequencies follow a magnetization curve with a significantly flatter temperature dependence and are far from that expected for a Heisenberg magnet with a

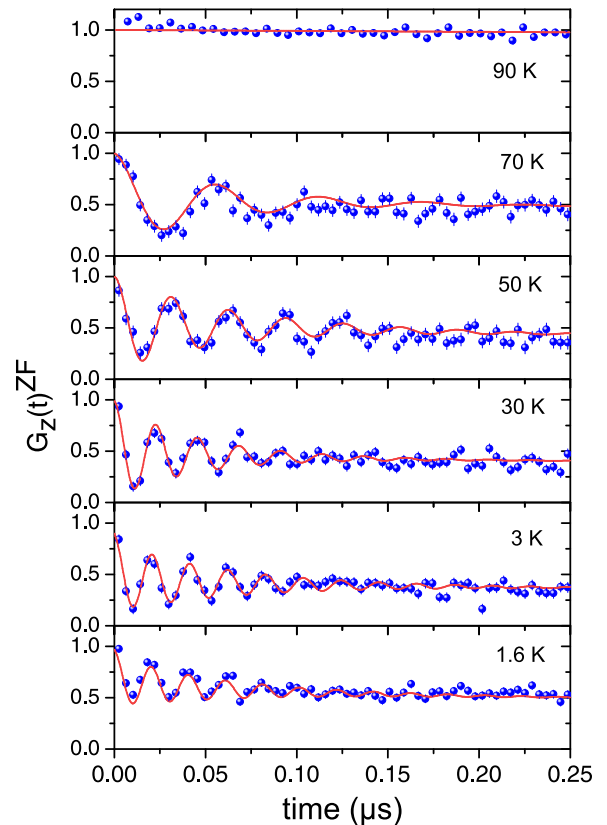


FIG. 11. ZF μSR spectra of $\text{Ni}_5\text{Sn}(\text{O}_2\text{BO}_3)_2$ for a time window of 0–0.25 μs . Spectra up to 5 μs are presented in the Supplemental Material [24].

critical exponent around 0.35. Flattened magnetization curves may be caused by distributions of exchange interactions. In our system, this is also supported by the strong damping of the spontaneous oscillations in ZF. It also shows that the magnetic fields traced by the muons are caused by a different spin ensemble than that responsible for the transferred hyperfine field at Sn.

As already expected from the wTF results, we need for the fit of the spectra additional signals. One is a temperature-independent undamped background signal [about 10% of total asymmetry] labeled BG in Eq. (1) and a damped one with about 20% partial asymmetry. This signal from the sample is best described by a generalized exponential damping function $G_z(t)_{\text{ge}}^{\text{ZF}} = \exp(-\lambda_{\text{ge}} t)^\beta$. Although down to 50 K the power factor β is 1 (i.e., pure Lorentzian damping), it decreases for lower temperatures (Fig. 12), a typical indication for spin-glass-like freezing accompanied by a wide distribution of correlation times. In parallel, we find an increase in the damping parameter λ_{ge} (presented in the Supplemental Material [24]). At 10 K and further below, we find a clear increase in this spin-glass-like signal at the expense of the rotating signal. The damping factor λ_{ge} shows a peak at 3 K. The variation of the partial asymmetries (a_{rot} , a_{ge} , and BG) is shown in the Supplemental Material [24]. We relate these changes to the anomaly found in the specific heat and the AC susceptibility peak around 5 K (Fig. 4).

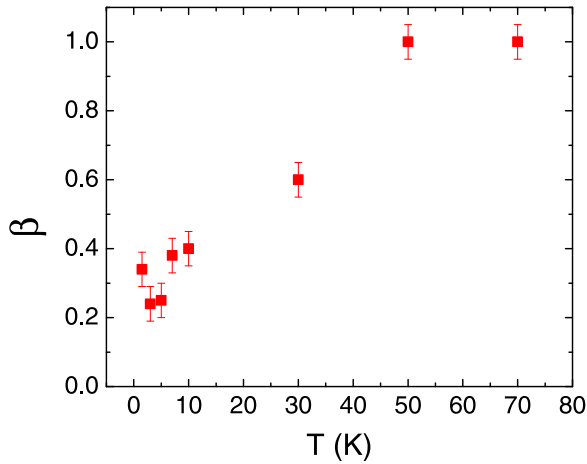


FIG. 12. Temperature dependence of power factor β of the generalized exponential damping function $G_z(t)_{ge}^{ZF} = \exp(-\lambda_{ge}t)^\beta$ [see Eq. (1)].

To summarize, we can see from μ SR a partial onset of static long-range magnetic order around 80 K: Only about 70% of the signal (i.e., about 80% of the sample volume) reveals resolved spontaneous oscillations associated with static long-range order. The rest of the signal assigned to the sample remains paramagnetic. At 30 K and below, the paramagnetic fraction indicates an onset of spin freezing. Below 10 K a depolarization typical for a spin-glass-like state is found. The related rise in asymmetry occurs at the expense of a part of the long-range ordered signal.

III. DISCUSSION

The structural difference of site-disordered and site-ordered $\text{Ni}_5\text{Sn}(\text{O}_2\text{BO}_3)_2$ ludwigites is only in ladder 4-2-4, specifically at site 4 where Sn and Ni ions are in 0.5:0.5 proportion with a random (disordered) and periodic (ordered) occupancy along the c axis as schematically represented in Fig. 2. As a consequence, different paths of magnetic interactions are allowed. The smallest intermetallic distances in ladder 4-2-4 usually makes possible direct exchange interactions that compete with superexchange ones. On the other hand, the absence of double-exchange interactions in these isomeric compounds with $S = 1$ magnetic moments provides a useful comparison. The different magnetic properties of site-disordered $\text{Ni}_5\text{Sn}(\text{O}_2\text{BO}_3)_2$ ludwigite here studied and of the site-ordered reported in Ref. [23] are summarized in Table II.

In site-disordered $\text{Ni}_5\text{Sn}(\text{O}_2\text{BO}_3)_2$ ludwigite, a ferrimagnetic order with predominant ferromagnetic interactions is established below 80 K as indicated by the negative Curie-Weiss temperature ($\theta_{\text{CW}} = -82$ K) and by the $M(H)$ and

specific-heat curves with ferromagnetic-like form. As indicated by μ SR experiments, this order is partial with only 70% of the signal corresponding to long-range magnetic order. This transition corresponds to the peak in the specific heat at 80 K. Mössbauer spectroscopy measurements were performed with Sn probe atoms, which occupy site 4, and the observed magnetic hyperfine splitting below 75 K can be associated with a long-range magnetic order of the 4-2-4 ladder in which the shortest distance between two Ni ions (2.797 Å) and the largest value of superexchange integrals calculated in Ref. [22] were found. The magnetic order occurs in two steps at 80 and 76 K, which is better observed by magnetization as seen from the insets of Figs. 3 and 4. Similar behavior has been found in the AC susceptibility of another site-disordered Ni ludwigite $\text{Ni}_5\text{Ti}(\text{O}_2\text{BO}_3)_2$ between 92 and 86 K [21]. These steps are not present in the AC and DC magnetization data of site-ordered $\text{Ni}_5\text{Sn}(\text{O}_2\text{BO}_3)_2$ ludwigite of Ref. [23], which shows magnetic order at 73 K. This comparison suggests that the stepwise magnetic-order behavior in site-disordered Ni ludwigites is originated in ladder 4-2-4 along the c axis. The random occupation of site 4 by Ni and Sn atoms results in Ni-rich and Ni-poor areas along this ladder, and these areas could order in different but close temperatures. Another effect of Ni-rich/Ni-poor areas on this site-disordered compound is the large increase in the coercive field at low temperatures in comparison with the site-ordered compound.

In addition, the Mössbauer spectra at low temperatures show an angle between the magnetic hyperfine field and the electric-field gradient main axes with $\theta \simeq 60^\circ$, that differs from $\theta = 0$ that was observed for $\text{Co}_5\text{Sn}(\text{O}_2\text{BO}_3)_2$ ludwigite [13]. Both compounds have magnetic anisotropy with the easy axis on the a - b plane, see the Supplemental Material [24]. The different angles between the magnetic hyperfine field and the electric-field gradient imply different angles of the easy axis against the a - b plane for the two compounds. Considering that the elongated octahedra around the four metal ion sites have their main axes pointing mainly along the b axis (see Fig. 1), $\theta = 0$ implies that the easy axis for $\text{Co}_5\text{Sn}(\text{O}_2\text{BO}_3)_2$ is the b axis as it is for $\text{Co}_3\text{O}_2\text{BO}_3$. For $\text{Ni}_5\text{Sn}(\text{O}_2\text{BO}_3)_2$, $\theta \simeq 60^\circ$ indicates an easy axis pointing mainly along the a axis as observed for $\text{Ni}_5\text{Ge}(\text{O}_2\text{BO}_3)_2$ [22]. From the μ SR results below 80 K, part of the sample (about 20%) reveals strongly damped paramagnetic behavior turning to spin-glass like at lower temperatures. This signal must be caused by ladder 3-1-3. In fact, the experimental results can be related to the group-theoretical analysis performed in Ref. [23]. It presents eight eigenvectors τ with the odd irreducible representations τ_1 , τ_3 , τ_5 , and τ_7 corresponding to full ordering of magnetic moments, which is not the case. However, for all even irreducible representations τ_2 , τ_4 , τ_6 , and τ_8 , the magnetic moments of the ions in site

TABLE II. Structural and magnetic parameters for $\text{Ni}_5\text{Sn}(\text{O}_2\text{BO}_3)_2$ ludwigite.

Sample	Occ. site 4	T_{N1} (K)	T_{N2} (K)	T_{SG} (K)	H_C (kOe) $T = 2$ K	H_{EB} (Oe) $T = 2$ K	M_{2K}^{FC} (emu/g) $H = 1000$ Oe	μ_{eff} μ_B	θ_{CW} (K)
PW	Disordered	80	50	5	13.8(5)	861 (10)	4.5(1)	5.28	-82.8
Ref. [23]	Ordered	73		15	1.3(5)		5.8(2)	5.05	-80

1 are disordered, whereas site 3 can have components in all (x , y , and z) directions. From this, one can understand why the magnetic moments in site 1 could remain paramagnetic. This model describes very well the paramagnetic and then the spin-glass-like fractions observed below 80 K by μ SR experiments. It is also interesting that the moments on sites 4 and 2 lie along the x - z plane for τ_2 and τ_6 and along y for τ_4 and τ_8 . From Mössbauer experiments and the magnetic anisotropy of the sample under applied magnetic fields, τ_2 and τ_6 appear to describe better the magnetic order.

The arrangement of magnetic moments is different below 50 K as indicated by the peak seen in the specific heat curves (Fig. 6), the inflection in the DC magnetization curve (the inset of Fig. 3), and the reduction of the value of the AC susceptibility (Fig. 4). From Mössbauer spectroscopy a continuous change in angle θ is observed in Table I. On the other hand, under an applied magnetic field of 9 T, a larger and narrower peak is observed in the specific heat (see the inset of Fig. 6). It could indicate a long-range order of the whole compound or a reorientation of the moments. Interestingly, in Ref. [23] the authors considered a model in which the magnetic order is on the plane formed by sites 2, 3, and 1, a model used also to describe the magnetic order in $\text{Co}_{4.76}\text{Al}_{1.24}(\text{O}_2\text{BO}_3)_2$ ludwigite [12]. They calculated the magnetic-ordering temperature of the subsystems: 4-2-4, 3-1-3, and 3-2-3. Subsystem 3-2-3 had the highest magnetic-ordering temperature with 52 K, and it coincides with the temperature of the highest and narrower peak observed in the specific heat under the applied field of 9 T. It is possible that under this high applied magnetic field the disordered spins of sites 1 and 3 get magnetically coupled to site 2, yielding 2D-like magnetic order on planes formed by sites 2, 3, and 1. This model is consistent with the dominant T^2 low-temperature specific heat at 9 T, which indicates magnon and phonon planar excitations.

Below 30 K, a partially spin-glass-like state develops as described in the μ SR section. The AC susceptibility data show a large peak at 5 K with a small dependence on frequency. The specific-heat curve in the zero magnetic field has a small anomaly around 5 K, which is not common in spin-glass systems. On the other hand, this anomaly disappears with applied magnetic fields, consistent with a spin-glass behavior.

Summarizing, one additional magnetic transition is observed, an increase in the coercive field and the appearance of the spontaneous exchange biaslike effect in this site-disordered compound when compared with the site-ordered counterpart. These differences are related to the increase in magnetic exchange paths where only direct exchange and superexchange are really competing.

IV. CONCLUSION

Magnetic oxyborates present a variety of interesting properties related to the low-dimensional cation substructures existing in these compounds. Magnetic frustrations and structural disorders play an important role in their magnetic properties. The different paths of magnetic interactions have a hierarchy describing three magnetic anomalies at 80, 50, and 5 K in site-disordered $\text{Ni}_5\text{Sn}(\text{O}_2\text{BO}_3)_2$ ludwigite. Predominantly ferromagnetic interactions at 80 K change to predominantly antiferromagnetic at 50 K. At lower temperatures, partial spin-glass freezing of moments and large magnetic frustrations are observed leading to coexisting spin-glass-like and long-range-ordered states at the lowest temperatures. Applied magnetic fields reduce frustration. A field of 9 T leads to magnetic order of the complete system at 51 K, and the incipient spin-glass-like state is suppressed. The change in predominance on the magnetic interactions at 50 K is particular of this ludwigite and can be explained by reduced anisotropy and structural disorder, highlighting the absence of double-exchange interactions.

ACKNOWLEDGMENTS

Support from the Brazilian agencies FAPERJ, CNPq, FAPESP (Grant No. 09/54082-2) and FAPES are gratefully acknowledged. A scholarship by FAPERJ supported F.J.L., E.S., E.B.-S., and F.J.L. were supported by DFG Project No. Li244/12-2. We also acknowledge LDRX-UFF (Universidade Federal Fluminense, Brazil) for use of their laboratory facilities. We are grateful to H. Luetkens for support during the experiments at the Swiss Muon Source $S\mu$ S, Paul Scherrer Institute, Villigen, Switzerland.

-
- [1] C. P. C. Medrano, D. C. Freitas, E. C. Passamani, J. A. L. C. Resende, M. Alzamora, E. Granado, C. W. Galdino, E. Baggio-Saitovitch, M. A. Continentino, and D. R. Sanchez, *Phys. Rev. B* **98**, 054435 (2018).
 - [2] A. Maignan, F. Lainé, A. Guesdon, S. Malo, F. Damay, and C. Martin, *J. Solid State Chem.* **246**, 209 (2017).
 - [3] P. Bordet and E. Suard, *Phys. Rev. B* **79**, 144408 (2009).
 - [4] J. Bartolomé, A. Arauzo, N. V. Kazak, N. B. Ivanova, S. G. Ovchinnikov, Y. V. Knyazev, and I. S. Lyubutin, *Phys. Rev. B* **83**, 144426 (2011).
 - [5] J. Sottmann, L. Nataf, L. Chaix, V. Pralong, and C. Martin, *J. Phys. Chem. C* **122**, 17042 (2018).
 - [6] E. Vallejo and M. Avignon, *J. Magn. Magn. Mater.* **435**, 33 (2017).
 - [7] F. Damay, J. Sottmann, F. Lainé, L. Chaix, M. Poinar, P. Beran, E. Elkaim, F. Fauth, L. Nataf, A. Guesdon *et al.*, *Phys. Rev. B* **101**, 094418 (2020).
 - [8] C. W. Galdino, D. C. Freitas, C. P. C. Medrano, R. Tartaglia, D. Rigitano, J. F. Oliveira, A. A. Mendonça, L. Ghivelder, M. A. Continentino, D. R. Sanchez, and E. Granado, *Phys. Rev. B* **100**, 165138 (2019).
 - [9] D. C. Freitas, C. P. C. Medrano, D. R. Sanchez, M. N. Regueiro, J. A. Rodríguez-Velamazán, and M. A. Continentino, *Phys. Rev. B* **94**, 174409 (2016).
 - [10] Y. Knyazev, N. Kazak, I. Nazarenko, S. Sofronova, N. Rostovtsev, J. Bartolome, A. Arauzo, and S. Ovchinnikov, *J. Magn. Magn. Mater.* **474**, 493 (2019).
 - [11] S. Kundu, B. Malik, D. K. Pattanayak, and V. K. Pillai, *ChemElectroChem* **5**, 1670 (2018).

- [12] C. P. C. Medrano, D. C. Freitas, E. C. Passamani, C. B. Pinheiro, E. Baggio-Saitovitch, M. A. Continentino, and D. R. Sanchez, *Phys. Rev. B* **95**, 214419 (2017).
- [13] Cynthia P. Contreras Medrano, D. C. Freitas, D. R. Sanchez, C. B. Pinheiro, G. G. Eslava, L. Ghivelder, and M. A. Continentino, *Phys. Rev. B* **91**, 054402 (2015).
- [14] D. C. Freitas, R. B. Guimaraes, D. R. Sanchez, J. C. Fernandes, M. A. Continentino, J. Ellena, A. Kitada, H. Kageyama, A. Matsuo, K. Kindo *et al.*, *Phys. Rev. B* **81**, 024432 (2010).
- [15] N. Ivanova, M. Platonov, Y. V. Knyazev, N. Kazak, L. Bezmaternykh, E. Eremin, and A. Vasiliev, *Low Temp. Phys.* **38**, 172 (2012).
- [16] J. C. Fernandes, R. B. Guimarães, M. A. Continentino, H. A. Borges, A. Sulpice, J.-L. Tholence, J. L. Siqueira, L. I. Zawislak, J. B. M. Da Cunha, and C. A. dos Santos, *Phys. Rev. B* **58**, 287 (1998).
- [17] D. C. Freitas, M. A. Continentino, R. B. Guimaraes, J. C. Fernandes, E. P. Oliveira, R. E. Santelli, J. Ellena, G. G. Eslava, and L. Ghivelder, *Phys. Rev. B* **79**, 134437 (2009).
- [18] E. Moshkina, S. Sofronova, A. Veligzhanin, M. Molokeev, I. Nazarenko, E. Eremin, and L. Bezmaternykh, *J. Magn. Magn. Mater.* **402**, 69 (2016).
- [19] L. Bezmaternykh, E. Kolesnikova, E. Eremin, S. Sofronova, N. Volkov, and M. Molokeev, *J. Magn. Magn. Mater.* **364**, 55 (2014).
- [20] J. Kumar, D. J. Mukkattukavil, A. Bhattacharyya, and S. Nair, *J. Phys.: Condens. Matter* **32**, 065601 (2019).
- [21] M. A. V. Heringer, D. C. Freitas, D. L. Mariano, E. Baggio-Saitovitch, M. A. Continentino, and D. R. Sánchez, *Phys. Rev. Mater.* **3**, 094402 (2019).
- [22] S. Sofronova, L. Bezmaternykh, E. Eremin, I. Nazarenko, N. Volkov, A. Kartashev, and E. Moshkina, *J. Magn. Magn. Mater.* **401**, 217 (2016).
- [23] S. Sofronova, L. Bezmaternykh, E. Eremin, A. Chernyshov, and A. Bovina, *Phys. Status Solidi B* **255**, 1800281 (2018).
- [24] See Supplemental Material at <http://link.aps.org/supplemental/10.1103/PhysRevB.103.064430> for details of the crystal structure and muon spin rotation and relaxation.
- [25] K. Momma and F. Izumi, *J. Appl. Crystallogr.* **44**, 1272 (2011).
- [26] L. J. Farrugia, *J. Appl. Crystallogr.* **45**, 849 (2012).
- [27] C. B. Hübschle, G. M. Sheldrick, and B. Dittrich, *J. Appl. Crystallogr.* **44**, 1281 (2011).
- [28] J. G. Cheng, G. Li, L. Balicas, J. S. Zhou, J. B. Goodenough, C. Xu, and H. D. Zhou, *Phys. Rev. Lett.* **107**, 197204 (2011).
- [29] A. G. Silva, K. S. Rodríguez, C. C. Medrano, G. S. G. Lourenço, M. Boldrin, E. Baggio-Saitovitch, and L. Bufaiçal, *J. Phys.: Condens. Matter* **33**, 065804 (2020).
- [30] Z. Klencsár, MOSSWINN 4.0I Manual, revision 03.02.2019, <http://www.mosswinn.com/downloads/mosswinn.pdf>.
- [31] N. N. Greenwood and T. C. Gibb, *Mössbauer Spectroscopy* (Chapman and Hall, London, 1971).